

Measurement of the top-quark mass in the $t\bar{t}$ dilepton channel using the full CDF Run II data set

T. Aaltonen,²¹ S. Amerio,^{39a,39b} D. Amidei,³¹ A. Anastassov,^{15,w} A. Annovi,¹⁷ J. Antos,¹² G. Apollinari,¹⁵ J. A. Appel,¹⁵ T. Arisawa,⁵² A. Artikov,¹³ J. Asaadi,⁴⁷ W. Ashmanskas,¹⁵ B. Auerbach,² A. Aurisano,⁴⁷ F. Azfar,³⁸ W. Badgett,¹⁵ T. Bae,²⁵ A. Barbaro-Galtieri,²⁶ V. E. Barnes,⁴³ B. A. Barnett,²³ P. Barria,^{41a,41c} P. Bartos,¹² M. Baucé,^{39a,39b} F. Bedeschi,^{41a} S. Behari,¹⁵ G. Bellettini,^{41a,41b} J. Bellinger,⁵⁴ D. Benjamin,¹⁴ A. Beretvas,¹⁵ A. Bhatti,⁴⁵ K. R. Bland,⁵ B. Blumenfeld,²³ A. Bocci,¹⁴ A. Bodek,⁴⁴ D. Bortoletto,⁴³ J. Boudreau,⁴² A. Boveia,¹¹ L. Brigliadori,^{6a,6b} C. Bromberg,³² E. Brucken,²¹ J. Budagov,¹³ H. S. Budd,⁴⁴ K. Burkett,¹⁵ G. Busetto,^{39a,39b} P. Bussey,¹⁹ P. Butti,^{41a,41b} A. Buzatu,¹⁹ A. Calamba,¹⁰ S. Camarda,⁴ M. Campanelli,²⁸ F. Canelli,^{11,ee} B. Carls,²² D. Carlsmith,⁵⁴ R. Carosi,^{41a} S. Carrillo,^{16,1} B. Casal,^{9j} M. Casarsa,^{48a} A. Castro,^{6a,6b} P. Catastini,²⁰ D. Cauz,^{48a,48b,48c} V. Cavaliere,²² A. Cerri,^{26,e} L. Cerrito,^{28,r} Y. C. Chen,¹ M. Chertok,⁷ G. Chiarelli,^{41a} G. Chlachidze,¹⁵ K. Cho,²⁵ D. Chokheli,¹³ A. Clark,¹⁸ C. Clarke,⁵³ M. E. Convery,¹⁵ J. Conway,⁷ M. Corbo,^{15,z} M. Cordelli,¹⁷ C. A. Cox,⁷ D. J. Cox,⁷ M. Cremonesi,^{41a} D. Cruz,⁴⁷ J. Cuevas,^{9,y} R. Culbertson,¹⁵ N. d'Ascenzo,^{15,v} M. Datta,^{15,hh} P. de Barbaro,⁴⁴ L. Demortier,⁴⁵ M. Deninno,^{6a} M. D'Errico,^{39a,39b} F. Devoto,²¹ A. Di Canto,^{41a,41b} B. Di Ruzza,^{15,p} J. R. Dittmann,⁵ S. Donati,^{41a,41b} M. D'Onofrio,²⁷ M. Dorigo,^{48a,48d} A. Driutti,^{48a,48b,48c} K. Ebina,⁵² R. Edgar,³¹ A. Elagin,⁴⁷ R. Erbacher,⁷ S. Errede,²² B. Esham,²² S. Farrington,³⁸ J. P. Fernández Ramos,²⁹ R. Field,¹⁶ G. Flanagan,^{15,t} R. Forrest,⁷ M. Franklin,²⁰ J. C. Freeman,¹⁵ H. Frisch,¹¹ Y. Funakoshi,⁵² C. Galloni,^{41a,41b} A. F. Garfinkel,⁴³ P. Garosi,^{41a,41c} H. Gerberich,²² E. Gerchtein,¹⁵ S. Giagu,^{46a} V. Giakoumopoulou,³ K. Gibson,⁴² C. M. Ginsburg,¹⁵ N. Giokaris,³ P. Giromini,¹⁷ V. Glagolev,¹³ D. Glenzinski,¹⁵ M. Gold,³⁴ D. Goldin,⁴⁷ A. Golossanov,¹⁵ G. Gomez,⁹ G. Gomez-Ceballos,³⁰ M. Goncharov,³⁰ O. González López,²⁹ I. Gorelov,³⁴ A. T. Goshaw,¹⁴ K. Goulianos,⁴⁵ E. Gramellini,^{6a} C. Grosso-Pilcher,¹¹ R. C. Group,^{51,15} J. Guimaraes da Costa,²⁰ S. R. Hahn,¹⁵ J. Y. Han,⁴⁴ F. Happacher,¹⁷ K. Hara,⁴⁹ M. Hare,⁵⁰ R. F. Harr,⁵³ T. Harrington-Taber,^{15,m} K. Hatakeyama,⁵ C. Hays,³⁸ J. Heinrich,⁴⁰ M. Herndon,⁵⁴ A. Hocker,¹⁵ Z. Hong,⁴⁷ W. Hopkins,^{15,f} S. Hou,¹ R. E. Hughes,³⁵ U. Husemann,⁵⁵ M. Hussein,^{32,cc} J. Huston,³² G. Introzzi,^{41a,41e,41f} M. Iori,^{46a,46b} A. Ivanov,^{7,o} E. James,¹⁵ D. Jang,¹⁰ B. Jayatilaka,¹⁵ E. J. Jeon,²⁵ S. Jindariani,¹⁵ M. Jones,⁴³ K. K. Joo,²⁵ S. Y. Jun,¹⁰ T. R. Junk,¹⁵ M. Kambeitz,²⁴ T. Kamon,^{25,47} P. E. Karchin,⁵³ A. Kasmai,⁵ Y. Kato,^{37,n} W. Ketchum,^{11,ii} J. Keung,⁴⁰ B. Kilminster,^{15,ee} D. H. Kim,²⁵ H. S. Kim,^{15,bb} J. E. Kim,²⁵ M. J. Kim,¹⁷ S. H. Kim,⁴⁹ S. B. Kim,²⁵ Y. J. Kim,²⁵ Y. K. Kim,¹¹ N. Kimura,⁵² M. Kirby,¹⁵ K. Knoepfel,¹⁵ K. Kondo,^{52,*} D. J. Kong,²⁵ J. Konigsberg,¹⁶ A. V. Kotwal,¹⁴ M. Kreps,²⁴ J. Kroll,⁴⁰ M. Kruse,¹⁴ T. Kuhr,²⁴ M. Kurata,⁴⁹ A. T. Laasanen,⁴³ S. Lammel,¹⁵ M. Lancaster,²⁸ K. Lannon,^{35,x} G. Latino,^{41a,41c} H. S. Lee,²⁵ J. S. Lee,²⁵ S. Leo,²² S. Leone,^{41a} J. D. Lewis,¹⁵ A. Limosani,^{14,s} E. Lipeles,⁴⁰ A. Lister,^{18,a} H. Liu,⁵¹ Q. Liu,⁴³ T. Liu,¹⁵ S. Lockwitz,⁵⁵ A. Loginov,⁵⁵ D. Lucchesi,^{39a,39b} A. Lucà,¹⁷ J. Lueck,²⁴ P. Lujan,²⁶ P. Lukens,¹⁵ G. Lungu,⁴⁵ J. Lys,²⁶ R. Lysak,^{12,d} R. Madrak,¹⁵ P. Maestro,^{41a,41c} S. Malik,⁴⁵ G. Manca,^{27,b} A. Manousakis-Katsikakis,³ L. Marchese,^{6a,jj} F. Margaroli,^{46a} P. Marino,^{41a,41d} K. Matera,²² M. E. Mattson,⁵³ A. Mazzacane,¹⁵ P. Mazzanti,^{6a} R. McNulty,^{27,i} A. Mehta,²⁷ P. Mehta,²¹ C. Mesropian,⁴⁵ T. Miao,¹⁵ D. Miettlicki,³¹ A. Mitra,¹ H. Miyake,⁴⁹ S. Moed,¹⁵ N. Moggi,^{6a} C. S. Moon,^{15,z} R. Moore,^{15,ff,gg} M. J. Morello,^{41a,41d} A. Mukherjee,¹⁵ Th. Müller,²⁴ P. Murat,¹⁵ M. Mussini,^{6a,6b} J. Nachtman,^{15,m} Y. Nagai,⁴⁹ J. Naganoma,⁵² I. Nakano,³⁶ A. Napier,⁵⁰ J. Nett,⁴⁷ C. Neu,⁵¹ T. Nigmanov,⁴² L. Nodulman,² S. Y. Noh,²⁵ O. Norriella,²² L. Oakes,³⁸ S. H. Oh,¹⁴ Y. D. Oh,²⁵ I. Oksuzian,⁵¹ T. Okusawa,³⁷ R. Orava,²¹ L. Ortolan,⁴ C. Pagliarone,^{48a} E. Palencia,^{9,e} P. Palni,³⁴ V. Papadimitriou,¹⁵ W. Parker,⁵⁴ G. Pauletta,^{48a,48b,48c} M. Paulini,¹⁰ C. Paus,³⁰ T. J. Phillips,¹⁴ G. Piacentino,^{15,q} E. Pianori,⁴⁰ J. Pilot,⁷ K. Pitts,²² C. Plager,⁸ L. Pondrom,⁵⁴ S. Poprocki,^{15,f} K. Potamianos,²⁶ A. Pranko,²⁶ F. Prokoshin,^{13,aa} F. Ptohos,^{17,g} G. Punzi,^{41a,41b} I. Redondo Fernández,²⁹ P. Renton,³⁸ M. Rescigno,^{46a} F. Rimondi,^{6a,*} L. Ristori,^{41a,15} A. Robson,¹⁹ T. Rodriguez,⁴⁰ S. Rolli,^{50,h} M. Ronzani,^{41a,41b} R. Roser,¹⁵ J. L. Rosner,¹¹ F. Ruffini,^{41a,41c} A. Ruiz,⁹ J. Russ,¹⁰ V. Rusu,¹⁵ W. K. Sakumoto,⁴⁴ Y. Sakurai,⁵² L. Santi,^{48a,48b,48c} K. Sato,⁴⁹ V. Saveliev,^{15,v} A. Savoy-Navarro,^{15,z} P. Schlabach,¹⁵ E. E. Schmidt,¹⁵ T. Schwarz,³¹ L. Scodellaro,⁹ F. Scuri,^{41a} S. Seidel,³⁴ Y. Seiya,³⁷ A. Semenov,¹³ F. Sforza,^{41a,41b} S. Z. Shalhout,⁷ T. Shears,²⁷ P. F. Shepard,⁴² M. Shimojima,^{49,u} M. Shochet,¹¹ I. Shreyber-Tecker,³³ A. Simonenko,¹³ K. Sliwa,⁵⁰ J. R. Smith,⁷ F. D. Snider,¹⁵ H. Song,⁴² V. Sorin,⁴ R. St. Denis,^{19,*} M. Stancari,¹⁵ D. Stentz,^{15,w} J. Strogas,³⁴ Y. Sudo,⁴⁹ A. Sukhanov,¹⁵ I. Suslov,¹³ K. Takemasa,⁴⁹ Y. Takeuchi,⁴⁹ J. Tang,¹¹ M. Tecchio,³¹ P. K. Teng,¹ J. Thom,^{15,f} E. Thomson,⁴⁰ V. Thukral,⁴⁷ D. Toback,⁴⁷ S. Tokar,¹² K. Tollefson,³² T. Tomura,⁴⁹ D. Tonelli,^{15,e} S. Torre,¹⁷ D. Torretta,¹⁵ P. Totaro,^{39a} M. Trovato,^{41a,41d} F. Ukegawa,⁴⁹ S. Uozumi,²⁵ F. Vázquez,^{16,l} G. Velev,¹⁵ C. Vellidis,¹⁵ C. Vernieri,^{41a,41d} M. Vidal,⁴³ R. Vilar,⁹ J. Vizán,^{9,dd} M. Vogel,³⁴ G. Volpi,¹⁷ P. Wagner,⁴⁰ R. Wallny,^{15,j} S. M. Wang,¹ D. Waters,²⁸ W. C. Wester III,¹⁵ D. Whiteson,^{40,c} A. B. Wicklund,² S. Wilbur,⁷ H. H. Williams,⁴⁰ J. S. Wilson,³¹ P. Wilson,¹⁵ B. L. Winer,³⁵ P. Wittich,^{15,f} S. Wolbers,¹⁵ H. Wolfe,³⁵ T. Wright,³¹ X. Wu,¹⁸ Z. Wu,⁵ K. Yamamoto,³⁷ D. Yamato,³⁷ T. Yang,¹⁵ U. K. Yang,²⁵ Y. C. Yang,²⁵ W.-M. Yao,²⁶ G. P. Yeh,¹⁵ K. Yi,^{15,m} J. Yoh,¹⁵ K. Yorita,⁵² T. Yoshida,^{37,k} G. B. Yu,¹⁴ I. Yu,²⁵ A. M. Zanetti,^{48a} Y. Zeng,¹⁴ C. Zhou,¹⁴ and S. Zucchelli^{6a,6b}

(CDF Collaboration)

¹*Institute of Physics, Academia Sinica, Taipei, Taiwan 11529, Republic of China*²*Argonne National Laboratory, Argonne, Illinois 60439, USA*

- ³University of Athens, 157 71 Athens, Greece
- ⁴Institut de Física d'Altes Energies, ICREA, Universitat Autònoma de Barcelona, E-08193 Bellaterra, Barcelona, Spain
- ⁵Baylor University, Waco, Texas 76798, USA
- ^{6a}Istituto Nazionale di Fisica Nucleare Bologna, I-40127 Bologna, Italy
- ^{6b}University of Bologna, I-40127 Bologna, Italy
- ⁷University of California, Davis, Davis, California 95616, USA
- ⁸University of California, Los Angeles, Los Angeles, California 90024, USA
- ⁹Instituto de Física de Cantabria, CSIC-University of Cantabria, 39005 Santander, Spain
- ¹⁰Carnegie Mellon University, Pittsburgh, Pennsylvania 15213, USA
- ¹¹Enrico Fermi Institute, University of Chicago, Chicago, Illinois 60637, USA
- ¹²Comenius University, 842 48 Bratislava, Slovakia; Institute of Experimental Physics, 040 01 Kosice, Slovakia
- ¹³Joint Institute for Nuclear Research, RU-141980 Dubna, Russia
- ¹⁴Duke University, Durham, North Carolina 27708, USA
- ¹⁵Fermi National Accelerator Laboratory, Batavia, Illinois 60510, USA
- ¹⁶University of Florida, Gainesville, Florida 32611, USA
- ¹⁷Laboratori Nazionali di Frascati, Istituto Nazionale di Fisica Nucleare, I-00044 Frascati, Italy
- ¹⁸University of Geneva, CH-1211 Geneva 4, Switzerland
- ¹⁹Glasgow University, Glasgow G12 8QQ, United Kingdom
- ²⁰Harvard University, Cambridge, Massachusetts 02138, USA
- ²¹Division of High Energy Physics, Department of Physics, University of Helsinki, FIN-00014, Helsinki, Finland; Helsinki Institute of Physics, FIN-00014 Helsinki, Finland
- ²²University of Illinois, Urbana, Illinois 61801, USA
- ²³The Johns Hopkins University, Baltimore, Maryland 21218, USA
- ²⁴Institut für Experimentelle Kernphysik, Karlsruhe Institute of Technology, D-76131 Karlsruhe, Germany
- ²⁵Center for High Energy Physics: Kyungpook National University, Daegu 702-701, Korea; Seoul National University, Seoul 151-742, Korea; Sungkyunkwan University, Suwon 440-746, Korea; Korea Institute of Science and Technology Information, Daejeon 305-806, Korea; Chonnam National University, Gwangju 500-757, Korea; Chonbuk National University, Jeonju 561-756, Korea; Ewha Womans University, Seoul 120-750, Korea
- ²⁶Ernest Orlando Lawrence Berkeley National Laboratory, Berkeley, California 94720, USA
- ²⁷University of Liverpool, Liverpool L69 7ZE, United Kingdom
- ²⁸University College London, London WC1E 6BT, United Kingdom
- ²⁹Centro de Investigaciones Energéticas Medioambientales y Tecnológicas, E-28040 Madrid, Spain
- ³⁰Massachusetts Institute of Technology, Cambridge, Massachusetts 02139, USA
- ³¹University of Michigan, Ann Arbor, Michigan 48109, USA
- ³²Michigan State University, East Lansing, Michigan 48824, USA
- ³³Institution for Theoretical and Experimental Physics, ITEP, Moscow 117259, Russia
- ³⁴University of New Mexico, Albuquerque, New Mexico 87131, USA
- ³⁵The Ohio State University, Columbus, Ohio 43210, USA
- ³⁶Okayama University, Okayama 700-8530, Japan
- ³⁷Osaka City University, Osaka 558-8585, Japan
- ³⁸University of Oxford, Oxford OX1 3RH, United Kingdom
- ^{39a}Istituto Nazionale di Fisica Nucleare, Sezione di Padova, I-35131 Padova, Italy
- ^{39b}University of Padova, I-35131 Padova, Italy
- ⁴⁰University of Pennsylvania, Philadelphia, Pennsylvania 19104, USA
- ^{41a}Istituto Nazionale di Fisica Nucleare Pisa, I-56127 Pisa, Italy
- ^{41b}University of Pisa, I-56127 Pisa, Italy
- ^{41c}University of Siena, I-56127 Pisa, Italy
- ^{41d}Scuola Normale Superiore, I-56127 Pisa, Italy
- ^{41e}INFN Pavia, I-27100 Pavia, Italy
- ^{41f}University of Pavia, I-27100 Pavia, Italy
- ⁴²University of Pittsburgh, Pittsburgh, Pennsylvania 15260, USA
- ⁴³Purdue University, West Lafayette, Indiana 47907, USA
- ⁴⁴University of Rochester, Rochester, New York 14627, USA
- ⁴⁵The Rockefeller University, New York, New York 10065, USA
- ^{46a}Istituto Nazionale di Fisica Nucleare, Sezione di Roma, I-00185 Roma, Italy
- ^{46b}Sapienza Università di Roma, I-00185 Roma, Italy
- ⁴⁷Mitchell Institute for Fundamental Physics and Astronomy, Texas A&M University, College Station, Texas 77843, USA

^{48a}*Istituto Nazionale di Fisica Nucleare Trieste, I-33100 Udine, Italy*
^{48b}*Gruppo Collegato di Udine, I-33100 Udine, Italy*
^{48c}*University of Udine, I-33100 Udine, Italy*
^{48d}*University of Trieste, I-34127 Trieste, Italy*
⁴⁹*University of Tsukuba, Tsukuba, Ibaraki 305, Japan*
⁵⁰*Tufts University, Medford, Massachusetts 02155, USA*
⁵¹*University of Virginia, Charlottesville, Virginia 22906, USA*
⁵²*Waseda University, Tokyo 169, Japan*
⁵³*Wayne State University, Detroit, Michigan 48201, USA*
⁵⁴*University of Wisconsin, Madison, Wisconsin 53706, USA*
⁵⁵*Yale University, New Haven, Connecticut 06520, USA*
 (Received 5 May 2015; published 6 August 2015)

We present a measurement of the top-quark mass in events containing two leptons (electrons or muons) with a large transverse momentum, two or more energetic jets, and a transverse-momentum imbalance. We use the full proton-antiproton collision data set collected by the CDF experiment during the Fermilab Tevatron Run II at center-of-mass energy $\sqrt{s} = 1.96$ TeV, corresponding to an integrated luminosity of 9.1 fb^{-1} . A special observable is exploited for an optimal reduction of the dominant systematic uncertainty, associated with the knowledge of the absolute energy of the hadronic jets. The distribution of this observable in the selected events is compared to simulated distributions of $t\bar{t}$ dilepton signal and background. We measure a value for the top-quark mass of 171.5 ± 1.9 (stat) ± 2.5 (syst) GeV/ c^2 .

DOI: 10.1103/PhysRevD.92.032003

PACS numbers: 14.65.Ha, 13.85.Qk, 13.85.Ni

*Deceased.

^aVisitor from University of British Columbia, Vancouver, BC V6T 1Z1, Canada.^bVisitor from Istituto Nazionale di Fisica Nucleare, Sezione di Cagliari, 09042 Monserrato (Cagliari), Italy.^cVisitor from University of California Irvine, Irvine, CA 92697, USA.^dVisitor from Institute of Physics, Academy of Sciences of the Czech Republic, 182 21, Czech Republic.^eVisitor from CERN, CH-1211 Geneva, Switzerland.^fVisitor from Cornell University, Ithaca, NY 14853, USA.^gVisitor from University of Cyprus, Nicosia CY-1678, Cyprus.^hVisitor from Office of Science, U.S. Department of Energy, Washington, DC 20585, USA.ⁱVisitor from University College Dublin, Dublin 4, Ireland.^jVisitor from ETH, 8092 Zürich, Switzerland.^kVisitor from University of Fukui, Fukui City, Fukui Prefecture, Japan 910-0017.^lVisitor from Universidad Iberoamericana, Lomas de Santa Fe, México, C.P. 01219, Distrito Federal.^mVisitor from University of Iowa, Iowa City, IA 52242, USA.ⁿVisitor from Kinki University, Higashi-Osaka City, Japan 577-8502.^oVisitor from Kansas State University, Manhattan, KS 66506, USA.^pVisitor from Brookhaven National Laboratory, Upton, NY 11973, USA.^qVisitor from Istituto Nazionale di Fisica Nucleare, Sezione di Lecce, Via Arnesano, I-73100 Lecce, Italy.^rVisitor from Queen Mary, University of London, London, E1 4NS, United Kingdom.^sVisitor from University of Melbourne, Victoria 3010, Australia.^tVisitor from Muons, Inc., Batavia, IL 60510, USA.^uVisitor from Nagasaki Institute of Applied Science, Nagasaki 851-0193, Japan.^vVisitor from National Research Nuclear University, Moscow 115409, Russia.^wVisitor from Northwestern University, Evanston, IL 60208, USA.^xVisitor from University of Notre Dame, Notre Dame, IN 46556, USA.^yVisitor from Universidad de Oviedo, E-33007 Oviedo, Spain.^zVisitor from CNRS-IN2P3, Paris, F-75205 France.^{aa}Visitor from Universidad Tecnica Federico Santa Maria, 110v Valparaiso, Chile.^{bb}Visitor from Sejong University, Seoul, South Korea.^{cc}Visitor from The University of Jordan, Amman 11942, Jordan.^{dd}Visitor from Universite Catholique de Louvain, 1348 Louvain-La-Neuve, Belgium.^{ee}Visitor from University of Zürich, 8006 Zürich, Switzerland.^{ff}Visitor from Massachusetts General Hospital, Boston, MA 02114 USA.^{gg}Visitor from Harvard Medical School, Boston, MA 02114, USA.^{hh}Visitor from Hampton University, Hampton, VA 23668, USA.ⁱⁱVisitor from Los Alamos National Laboratory, Los Alamos, NM 87544, USA.^{jj}Visitor from Università degli Studi di Napoli Federico I, I-80138 Napoli, Italy.

I. INTRODUCTION

In the standard model (SM) of particle physics, quark masses are proportional to their unknown Yukawa couplings to the Higgs field. Consequently, the masses are free parameters of the theory and must be determined experimentally. Precise measurements of the top-quark mass (M_{top}) provide critical inputs to global fits of the electroweak parameters for checking the internal consistency of the SM [1] and for understanding the stability of the electroweak vacuum at high energies [2].

At the Fermilab Tevatron and the LHC colliders, measurements by the ATLAS, CDF, CMS, and D0 collaborations have given consistent results, whose combination has determined M_{top} with a relative uncertainty of 0.44% [3]. The recent Tevatron combination performed by CDF and D0 collaborations improved the relative uncertainty to 0.37% [4]. All mass measurements in these combinations were done analyzing events where the top quarks are produced in pairs ($t\bar{t}$). The top quark decays almost exclusively into a W boson and a b quark [5] and, depending on the decay modes of the two resulting W bosons, top quark-pair events yield final states with either 0, 1, or 2 charged leptons. To improve the overall precision, the top-quark mass should be measured independently in all decay channels. In the present analysis, we consider the events in the dilepton final state, which is defined by the presence of two oppositely charged leptons (electrons or muons), two or more jets, and a large imbalance in the total transverse momentum from the two neutrinos associated with the charged leptons (“ $t\bar{t}$ dilepton events” or “dilepton channel”).

At the Tevatron, the most accurate M_{top} measurements in the dilepton channel [6,7] use methods of full or partial reconstruction of the top-quark events. In these analyses, the systematic uncertainty dominates over the statistical one with a large contribution of the jet-energy scale (JES) uncertainty. Measurements in the other final states reduce the JES systematic uncertainty by constraining the mass of the final-state jet pair to match the W -boson mass. This constraint permits a precise calibration of the calorimeter JES [8–10]. Since dilepton $t\bar{t}$ events do not contain jets from W decays, we devise a new method to reduce the impact of the JES uncertainty on the measurement result. In the past, CDF developed two methods to reconstruct the top-quark mass using only quantities with minimal dependence on the JES. One measurement exploited the transverse decay length of b -tagged jets [11] and another the transverse momentum of electrons and muons from W -boson decays to determine the top-quark mass [11,12]. These methods decreased the systematic uncertainty stemming from the JES uncertainty, but suffered from an increase of the statistical uncertainty due to their low sensitivity to the top-quark mass. In the current analysis, we combine two reconstruction methods, one with a strong dependence and one with a minimal dependence on JES. The combined method simultaneously optimizes the effect of the statistical

and systematic uncertainties delivering a result with a minimal total uncertainty.

This paper reports on the final CDF M_{top} measurement in the dilepton channel performed with proton-antiproton collision data at $\sqrt{s}=1.96\text{TeV}$, collected at the Tevatron with the CDF II detector [13]. The measurement uses the full CDF Run II data set accumulated between March 2002 and September 2011 and corresponds to an integrated luminosity of 9.1fb^{-1} . The results supersede those of Ref. [6] by exploiting an improved analysis technique and an additional integrated luminosity of about 3fb^{-1} .

II. DETECTOR, DATA SAMPLE AND EVENT SELECTION

The CDF II detector is a general-purpose apparatus [13] designed to detect the products of $p\bar{p}$ collisions at the Tevatron. It consists of a magnetic spectrometer surrounded by calorimeters and muon detectors. The spectrometer has a charged-particle tracking system consisting of a silicon microstrip tracker and a drift chamber. The tracking system is immersed in the 1.4 T magnetic field of a solenoid aligned with the beams. Segmented towers of electromagnetic and hadronic sampling calorimeters, located outside the solenoid, measure particle energies. A set of drift chambers and scintillation counters surrounds the calorimeters and detects muons. The detector has an approximate cylindrical geometry around the Tevatron beam line, which makes it convenient to use a cylindrical coordinate system [14] to describe the kinematic properties of reconstructed events.

The data are collected with an inclusive online event selection (trigger) that requires an electron (or a muon) with transverse energy $E_T > 18\text{GeV}$ (transverse momentum $p_T > 18\text{GeV}/c$) in the central pseudorapidity region ($|\eta| < 1.1$) of the detector. Off-line, the sample is further selected using the criteria developed for the $t\bar{t}$ cross section measurement in the dilepton channel [15]. In this analysis we introduce additional requirements to improve event modeling and to reduce the total background.

For the selection of events we require the presence of two oppositely charged leptons (ℓ), with $E_T > 20\text{GeV}$ for electrons or $p_T > 20\text{GeV}/c$ for muons, at least one of which must be isolated [16] and detected in the central region of the detector ($|\eta| < 1.1$). We further require large missing transverse energy [17], $\cancel{E}_T > 25\text{GeV}$, and at least two jets with $E_T > 15\text{GeV}$ and $|\eta| < 2.5$. To detect jets we look for clusters of energy in the calorimeter using a cone algorithm with radius $R = \sqrt{(\Delta\eta)^2 + (\Delta\phi)^2} = 0.4$ [18], where ϕ denotes the azimuthal angle. Jet energies are corrected for instrumental effects [19]. In events in which \cancel{E}_T originates from mismeasurements of the leptons or jets, the azimuthal angle between the \cancel{E}_T vector and the direction of the mismeasured object is typically small. To suppress this instrumental background, we increase the \cancel{E}_T requirement to $\cancel{E}_T > 50\text{GeV}$ for events where $\Delta\phi$ between the

directions of \vec{E}_T and at least one of the reconstructed leptons or jets is less than 20° . One of the main backgrounds is due to events in which a Z boson is produced in association with jets and decays to an electron or muon pair ($Z \rightarrow ee, \mu\mu + \text{jets}$). These events may feature large \vec{E}_T due to a mismeasurement of the leptons or jets. Therefore, a supplementary requirement is applied to e^+e^- and $\mu^+\mu^-$ events when the dilepton mass is within $15 \text{ GeV}/c^2$ of the known Z -boson mass [5]. For these events, we require a \vec{E}_T significance [20] in excess of $4 \text{ GeV}^{1/2}$. Since the products of $t\bar{t}$ decays have large transverse energies, further background suppression is achieved by requiring $H_T > 200 \text{ GeV}$ [21]. Another large source of background is due to events in which a W boson produced in association with jets ($W + \text{jets}$) yields a single lepton in the final state, where one of the jets is misidentified as a second lepton (“ $W + \text{jets}$ fakes”). We find that approximately half of these events feature a small distance in the η - ϕ space between the fake lepton and the axis of one of the jets (j), $\Delta R_{\ell j} = \sqrt{(\Delta\eta_{\ell j})^2 + (\Delta\phi_{\ell j})^2}$. To reject this background we require $\Delta R_{\ell j}$ to be greater than 0.2 for all possible pairings between leptons and jets in the event.

To obtain the most probable value of the top-quark mass per event (M_t^{reco}), we use a kinematic reconstruction method. This method calculates M_t^{reco} using all of the available experimental event information and has optimal sensitivity to M_{top} . From simulation, 6% of background events have M_t^{reco} larger than $250 \text{ GeV}/c^2$, while only about 0.5% of signal, simulated with M_{top} between 160 to $185 \text{ GeV}/c^2$, contributes to this region. In the analysis, we reject the events with $M_t^{\text{reco}} > 250 \text{ GeV}/c^2$. Finally, the dilepton invariant mass is required to be larger than $10 \text{ GeV}/c^2$ to suppress events from the decays of low-mass dimuon resonances and to improve the background modeling. In total we have 520 $t\bar{t}$ dilepton candidates that pass the selection requirements.

The sensitivity of the measurement is improved by analyzing separately events with a jet identified as originating from the fragmentation a bottom quark (b -tagged). We divide the event sample into two independent subsamples. The first subsample (b -tagged sample) contains events with at least one b -jet tagged using the secondary vertex (SECVTX) b -tagging algorithm [22]. This algorithm uses information from the displacement of secondary vertices relative to the primary event vertices to “tag” b -hadron decays. The second subsample contains events in which no b -tag is found (nontagged sample).

The PYTHIA [23] Monte Carlo (MC) program with CTEQ5L [24] parton distribution functions is used to generate samples of $t\bar{t}$ events with various top-quark masses. All MC samples are generated in combination with a detailed simulation of the CDF II detector [25]. Depending on the process, backgrounds are modeled using simulated or experimental data. The MC samples of diboson events (WW , WZ , and ZZ) are obtained using

TABLE I. Number of expected and observed events in the b -tagged and nontagged samples.

Source	b -tagged sample	Nontagged sample
WW	0.6 ± 0.2	16.4 ± 3.6
WZ	0.1 ± 0.0	5.2 ± 1.0
ZZ	0.2 ± 0.1	3.0 ± 0.5
Drell-Yan	4.4 ± 0.4	51.2 ± 8.0
Fakes	8.6 ± 2.7	21.4 ± 6.2
Total background	13.9 ± 2.8	97.2 ± 14.5
$t\bar{t}$ ($\sigma = 7.4 \text{ pb}$)	227.2 ± 16.2	173.2 ± 13.3
Total SM expectation	241.1 ± 16.4	270.3 ± 26.4
Observed	230	290

PYTHIA whereas the Drell-Yan events ($Z/\gamma^* + \text{jets}$, $Z/\gamma^* \rightarrow ee, \mu\mu, \tau\tau$) are generated with the ALPGEN program [26] interfaced to PYTHIA for showering and hadronization. A detailed description of the CDF MC procedures and samples is provided in Ref. [27]. The background originating from events in which a jet is misidentified as a lepton is modeled with $W + \text{jets}$ data. The composition of the data sample is estimated using the methods described in Ref. [15]. Table I summarizes the expected and observed $t\bar{t}$ signal and background yields. The signal yield is calculated assuming 7.4 pb for the $t\bar{t}$ production cross section. The Drell-Yan and $W + \text{jets}$ (“fake”) events are the main sources of contamination. Table I shows excellent agreement between expected and observed event yields.

III. METHODOLOGY

The template technique [28] used in this analysis estimates the top-quark mass by performing a fit of the distribution of an observable to a sum of signal and background contributions. This method can be applied to any observable whose distribution depends on M_{top} . However, the choice of the observable has direct impact on the precision of the measurement. For this analysis, we develop a variable that is expected to achieve a minimal measurement uncertainty. We start from two initial observables: the first observable is M_t^{reco} , which is computed using the “neutrino ϕ -weighting method” [29]. To account for the unconstrained kinematics of the top-quark decay, we scan over the phase space of the azimuthal angles of both neutrino momenta and for each point of this two-dimensional scan we reconstruct the top-quark mass by minimizing a χ^2 function for the $t\bar{t}$ final state hypothesis. Following the scan, we assign χ^2 -dependent weights to the solutions in order to identify a preferred M_t^{reco} for each event. Since this method uses all of the event information, including the jet energies, the reconstructed mass strongly depends on the calorimeter JES.

To reduce this systematic dependence, we consider a second observable that is insensitive to the JES. Testing a number of observables defined without using any information about jet energies, we choose the one that has the best sensitivity to M_{top} . This observable, denoted as

“alternative” mass ($M_{\ell b}^{\text{alt}}$), is defined according to the following formula:

$$M_{\ell b}^{\text{alt}} = c^2 \sqrt{\frac{\langle \ell_1, b_1 \rangle \cdot \langle \ell_2, b_2 \rangle}{E_{b_1} \cdot E_{b_2}}}, \quad (1)$$

where ℓ_1 and ℓ_2 are the four-momenta of leptons, and b_1 and b_2 are the four-momenta of the two highest- E_T (“leading”) jets, which are defined as for massless particles, with energies E_{b_1} and E_{b_2} . The quantity $\langle l, b \rangle$ indicates the scalar product of the ℓ and b four-vectors. The jet energies E_{b_1} and E_{b_2} appear in the denominator of Eq. (1) to cancel the $M_{\ell b}^{\text{alt}}$ JES-dependence of the leading jets, present in the numerator.

The use of the two leading jets in Eq. (1) is justified because in about 78% of the selected $t\bar{t}$ events the two leading jets originate from the hadronization of the two b quarks in the $t\bar{t}$ decay, according to simulation. We use the same index (1 or 2) to indicate a lepton and a jet that are assumed to originate from the decay of the same top quark. To choose between the two possible pairings of leptons and b -jets, we select the configuration with the maximum value of the scalar products $\langle c_{l_1}, c_{b_1} \rangle + \langle c_{l_2}, c_{b_2} \rangle$ where c is a unit vector collinear with the lepton or b -jet directions and the indexes l_1 and b_1 (l_2 and b_2) correspond to the lepton and b -jet in the first (second) pair. From simulation, we estimate that this lepton-to-jet pairing criterion selects the right pairing in $61 \pm 1\%$ of the cases. Other pairing criteria provide higher pairing efficiency of about 70%. However, these criteria use JES-dependent variables that create undesirable correlations between $M_{\ell b}^{\text{alt}}$ and M_t^{reco} .

We define the “hybrid” variable M^{hyb} ,

$$M^{\text{hyb}} = w \cdot M_t^{\text{reco}} + (1 - w) \cdot M_{\ell b}^{\text{alt}}, \quad (2)$$

where w is a weighting parameter between 0 and 1. The statistical and systematic uncertainties of the measurement depend on the choice of the w parameter. *A priori*, we choose the value of w that gives the smallest combined statistical and systematic uncertainty based on simulation. In order to find the optimal value of w , we scan the [0,1] interval in steps of 0.05. For every point of the scan, we define the mass fit using the signal and background templates for M^{hyb} and evaluate the uncertainties.

Signal templates for M^{hyb} are formed separately for b -tagged and nontagged events from $t\bar{t}$ samples generated for top-quark masses M_{top} in the range from 160 to 185 GeV/ c^2 with a 1 GeV/ c^2 step. The probability density functions (p.d.f.’s) of the signal, which express the probability of getting any M^{hyb} value in $t\bar{t}$ events with given M_{top} , are obtained as parametrizations of the corresponding templates. We parametrize the templates using a sum of two Landau and one Gaussian probability distribution functions. The parameters of these p.d.f.’s depend linearly on M_{top} . The background templates are derived separately for

b -tagged and nontagged events by adding diboson, fake, and Drell-Yan templates that are normalized to the expected rates reported in Table I. The background p.d.f.’s are obtained from a likelihood fit of the combined background templates, performed in the same way as for the signal templates, but without any dependence on the top-quark mass.

To measure M_{top} we perform a likelihood fit of the unbinned data distributions to a weighted sum of signal and background p.d.f.’s. The mass returned by the fit corresponds to the maximum of a likelihood function ($\mathcal{L}^{\text{total}}$) defined as the product of independent likelihood functions obtained for b -tagged and nontagged subsamples $\mathcal{L}^{\text{total}} = \mathcal{L}^{\text{tag}} \cdot \mathcal{L}^{\text{nontag}}$. The terms \mathcal{L}^{tag} and $\mathcal{L}^{\text{nontag}}$ represent the probabilities that the M^{hyb} distribution observed in data comes from a mixture of background events and $t\bar{t}$ dilepton events with an assumed top-quark mass M_{top} . The \mathcal{L}^{tag} and $\mathcal{L}^{\text{nontag}}$ form is similar to the likelihood function used in Refs. [29,30] and can be written as

$$\mathcal{L}^i = \mathcal{L}_{\text{constr}}^{\text{bg}}(n_b^i) \cdot \mathcal{L}_{\text{stat}}(N^i | n_s^i + n_b^i) \cdot \prod_{k=1}^{N^i} \mathcal{L}_{\text{evt}}^k(M^{\text{hyb},k} | M_{\text{top}}, n_s^i, n_b^i), \quad (3)$$

where N^i is the number of events in the corresponding subsample i . Using the signal and background p.d.f.’s, the likelihood term $\mathcal{L}_{\text{evt}}^k$ represents the probability for an event k with mass $M^{\text{hyb},k}$ to be observed in sample i where n_s^i and n_b^i events are expected for signal and background, respectively. The term $\mathcal{L}_{\text{stat}}$ gives the probability of observing N^i events in the sample, according to a Poisson distribution, while $\mathcal{L}_{\text{constr}}^{\text{bg}}$ constrains the number of background events in the corresponding subsample to the value shown in Table I. Having as inputs the M^{hyb} values observed in data, the signal and background p.d.f.’s, and the expected background, the likelihood fit returns the estimated top-quark mass (M_t^{fit}) and the estimated number of signal and background events.

Since M^{hyb} depends on w , the likelihood fit is different at each point of the w -scan. The correctness of these w -dependent fits is checked with simulated experiments (“pseudoexperiments” or PE’s) performed on samples of MC events with given input top-quark mass ($M_{\text{top}}^{\text{inp}}$). In every PE we draw the number of signal and background events according to Poisson distributions with means given in Table I and then draw values of M^{hyb} according to the corresponding signal and background templates. PE’s obtained in this way are used in our check of likelihood fitting. They confirm that M_t^{fit} is an unbiased estimate of M_{top} and its uncertainty is also correctly estimated.

In order to choose which w -dependent likelihood fit is to be applied to the data, we estimate the uncertainties as functions of w . We define the expected statistical uncertainty as the average statistical uncertainty in PE’s with

$M_{\text{top}}^{\text{inp}} = 172.5 \text{ GeV}/c^2$. To evaluate the JES systematic uncertainty, we test the impact of the uncertainties associated with the following effects: nonuniformity in calorimeter response as a function of $|\eta|$, multiple $p\bar{p}$ interactions in the same collision, hadronic jet-energy scale, energy contribution to the event from the fragments of the interacting proton and antiproton (underlying event), and out-of-cone energy lost in the energy-clustering procedure. We vary the corresponding JES parameters [19] by ± 1 standard deviation of their estimates and build alternative templates for both simulated signal and background events. These templates are used to generate PE's and the average deviations of the results from those obtained with default templates are interpreted as the corresponding systematic uncertainties. The individual uncertainties are then summed in quadrature to obtain the combined JES uncertainty.

Using the PE's method, we study the systematic uncertainties from sources other than JES for a few values of w . We estimate these effects by calculating the average deviations between the results of PE's performed with default and modified templates. The modified templates are derived by using event samples generated with variations of the relevant parameters within their uncertainties. We estimate the modeling uncertainty that stems from the difference between leading-order (LO) and next-to-leading-order (NLO) quantum chromodynamics (QCD) calculations by comparing MC samples from LO and NLO generators (PYTHIA and POWHEG). The uncertainty arising from the choice of the MC hadronization model and MC generator is estimated by comparing samples generated by using PYTHIA and HERWIG [31] computer codes. The systematic effect due to the lepton-energy scale uncertainty is evaluated by varying the electron energy and muon momentum scales. The systematic uncertainty associated with background modeling accounts for the variations of the background template shapes, the background composition and the total background normalization. The systematic effect due to the imperfect modeling of the initial-state and final-state gluon radiation is estimated by varying the PYTHIA parameters that control the amount of these radiations. To estimate the systematic effect due to the top-quark production mechanism (gg fraction) we vary the relative fractions of $q\bar{q} \rightarrow t\bar{t}$ and $gg \rightarrow t\bar{t}$ subprocesses in the PYTHIA model by reweighting the gluon fraction from 5% to 20%. We take into account the additional uncertainty on the b -jet-energy scale due to the difference in calorimeter response to jets from light quarks and b quarks and the imperfect modeling of the b -quark fragmentation and b -hadron decay branching fractions. The systematic effect due to the difference in the luminosity profile between data and MC is estimated. The color reconnection (CR) systematic uncertainty [32] is evaluated by comparing PYTHIA MC samples generated with and without CR effects. We take into account the systematic effect stemming from the limited size of the MC samples. We estimate the systematic uncertainty

due to parton distribution functions (PDFs) by comparing results from two different PDF families, varying the QCD scale, and propagating the uncertainties arising from the global fit of the CTEQ6M [33] functions. The systematic uncertainty related to the modeling of the b -tagging efficiency is also estimated. Details of the systematic uncertainty estimation are in Ref. [34].

The combined systematic uncertainty generated by sources other than JES ("non-JES uncertainty") is calculated as the sum in quadrature of these uncertainties. To estimate the non-JES systematic uncertainty for any value of w , we use cubic spline interpolations. The obtained values of the expected statistical, JES, non-JES, and total uncertainties are shown as functions of w in Fig. 1. The expected statistical and JES uncertainties are changing in the opposite direction as w varies between 0 and 1 while the non-JES uncertainty shows a slow falling dependence. The expected total uncertainty is estimated as the sum in quadrature of the statistical, JES and non-JES uncertainties and has a minimum in the interval between 0.5 and 0.7.

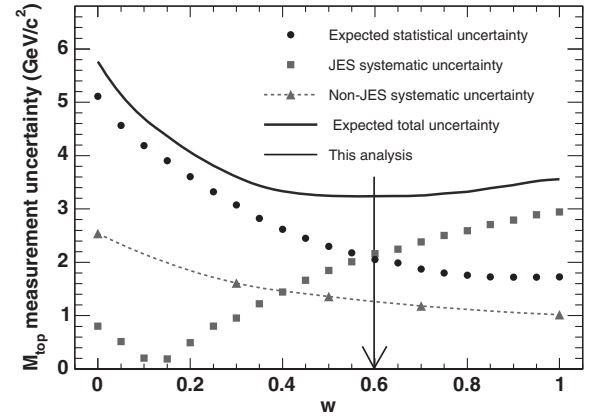


FIG. 1. Uncertainties in the measurement of M_{top} as a function of w . The arrow at $w = 0.6$ shows the minimum of the expected total uncertainty.

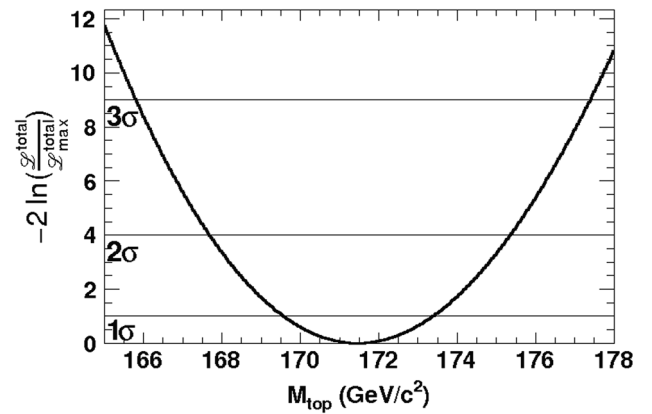


FIG. 2. Observed shape of $-2 \ln(\mathcal{L}^{\text{total}}/\mathcal{L}^{\text{total}_{\text{max}}})$ as a function of the top-quark mass. Horizontal lines show the values corresponding to one, two, and three standard-deviation uncertainties.

TABLE II. Summary of uncertainties.

Source	Uncertainty (GeV/ c^2)
Jet-energy scale	2.2
NLO effects	0.7
Monte Carlo generators	0.5
Lepton-energy scale	0.4
Background modeling	0.4
Initial- and final-state radiation	0.4
gg fraction	0.3
b -jet-energy scale	0.3
Luminosity profile	0.3
Color reconnection	0.2
MC sample size	0.2
Parton distribution functions	0.2
b -tagging	0.1
Total systematic uncertainty	2.5
Statistical uncertainty	1.9
Total	3.2

For the data fit, we use $w = 0.6$. We observe a 9% improvement in the total uncertainty in the case of $w = 0.6$ with respect to using only the reconstructed M_t^{reco} analysis ($w = 1$).

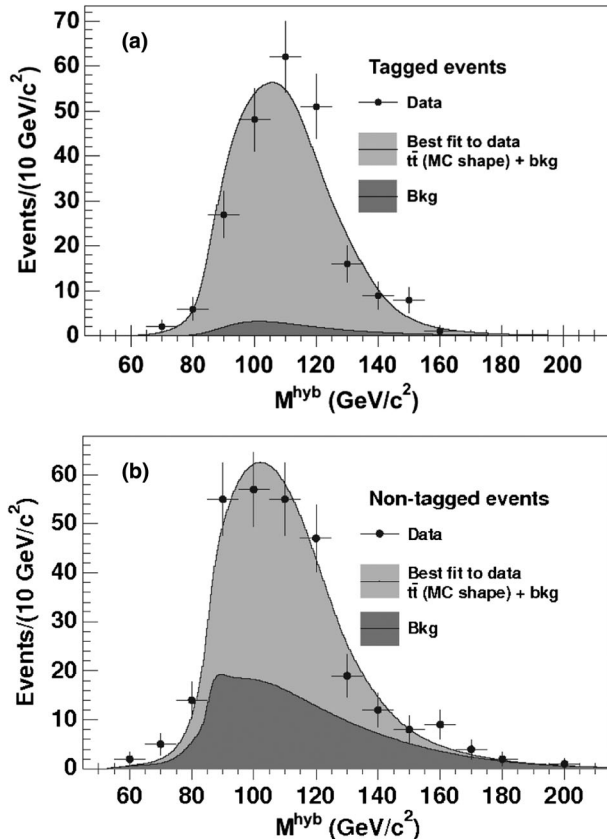


FIG. 3. Distribution of the reconstructed variable M^{hyb} . The figure shows the data (points), the background (dark gray) and signal (at measured M_{top}) plus background (light gray) p.d.f.'s, normalized accordingly to the fit result. Plots (a) and (b) correspond to b -tagged and nontagged subsamples.

Although $M_{\ell b}^{\text{alt}}$ does not depend explicitly on JES, the M_{top} measurement using only $M_{\ell b}^{\text{alt}}$ (points with $w = 0$ in Fig. 1) is still affected by the JES uncertainty because the JES impacts the event selection. When varying the JES, the change in event sample accepted by the selection criteria on variables that depend on jet energies generates a change in the $M_{\ell b}^{\text{alt}}$ distribution that affects the M_{top} measurement. We find that by varying the JES, opposite systematic shifts are induced in M_t^{reco} and $M_{\ell b}^{\text{alt}}$. These systematic shifts bias the M_{top} measurement in opposite directions minimizing the JES uncertainty at $w = 0.12$. This minimum depends only on the variables choice, M_t^{reco} and $M_{\ell b}^{\text{alt}}$, and their sensitivity to M_{top} . If the sample size would be large such that the statistical uncertainty could be neglected, the $w = 0.12$ choice would be optimal for this analysis. In that scenario, the JES uncertainty would approximate zero and the non-JES uncertainty would remain as the major contributor to the total measurement uncertainty.

IV. RESULT

With $w = 0.6$ the fit to the data yields $M_{\text{top}} = 171.5 \pm 1.9$ GeV/ c^2 including statistical uncertainties only. The normalized negative log-likelihood function versus the

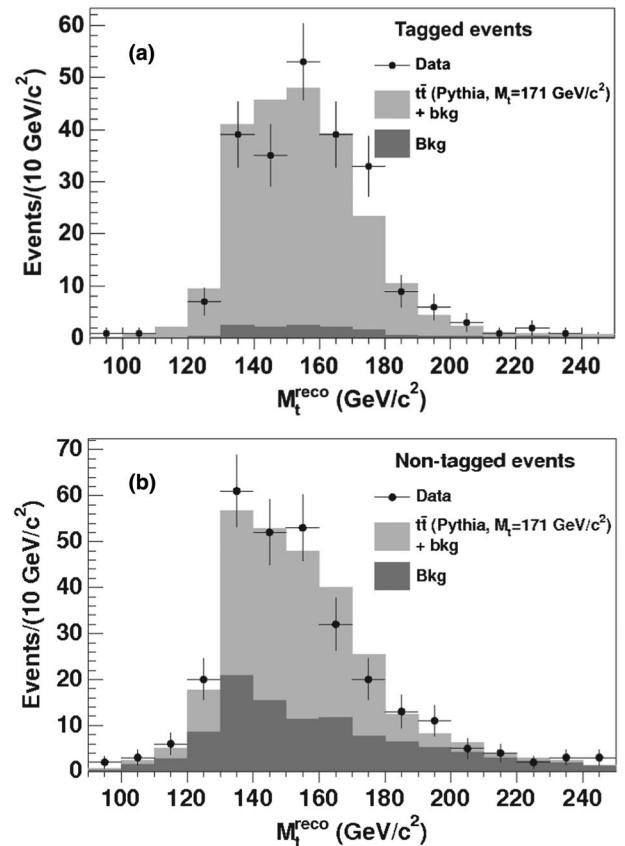


FIG. 4. Distributions of reconstructed mass M_t^{reco} overlaid with the background (dark gray) and signal plus background (light gray) histograms in the (a) b -tagged and (b) nontagged subsamples.

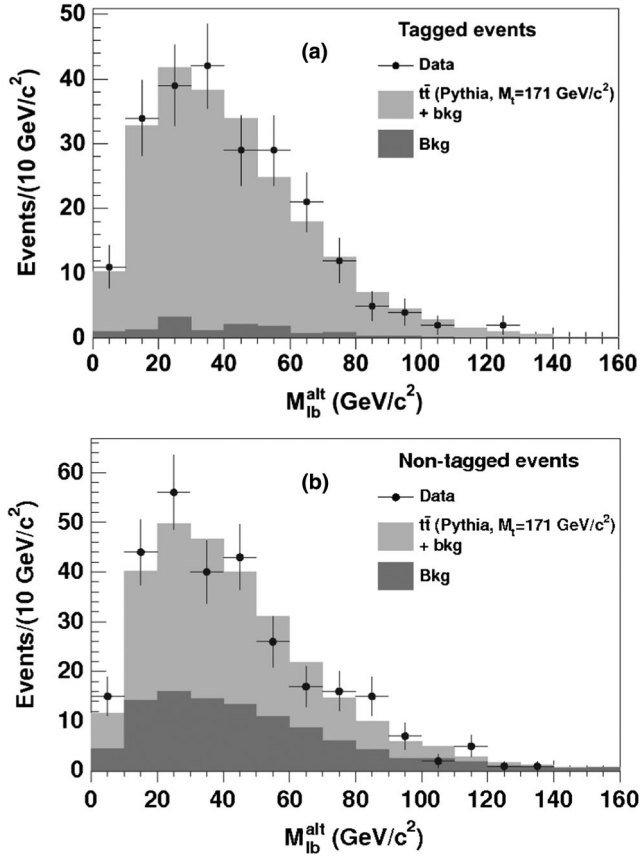


FIG. 5. Distributions of reconstructed mass M_{lb}^{alt} overlaid with the background (dark gray) and signal plus background (light gray) histograms in the (a) b -tagged and (b) nontagged subsamples.

top-quark mass is shown in Fig. 2. Its shape approximates a parabola and the horizontal lines show the values of likelihood ratios corresponding to one, two, and three standard-deviation (σ) uncertainties.

The individual systematic uncertainties affecting the M_{top} measurement are listed in Table II. The total systematic uncertainty, obtained by adding individual components in quadrature, is $2.5 \text{ GeV}/c^2$. The statistical and total systematic uncertainties combined in quadrature amount to a total uncertainty of $3.2 \text{ GeV}/c^2$.

Figure 3 shows the M^{hyb} distributions for b -tagged and nontagged events. We superimpose the data points to the expected signal and background distributions normalized to the numbers of events returned by the fit. The signal distribution corresponds to the measured value of M_{top} .

Similar plots for the variables M_t^{reco} and $M_{\ell b}^{\text{alt}}$ are shown in Figs. 4 and 5. All plots are normalized to the numbers of events returned by the fit. The top-quark mass value of

$171 \text{ GeV}/c^2$, closest to the value returned by the data fit, is used for the signal histogram. The p -values for the M_t^{reco} distributions are 71% and 91% for the b -tagged and nontagged subsamples. For the $M_{\ell b}^{\text{alt}}$ distributions, the p -values are 96% and 55% for the b -tagged and nontagged subsamples. An excellent agreement between data and the simulated distributions is observed.

V. SUMMARY

In conclusion, we present a measurement of the top-quark mass with $t\bar{t}$ dilepton events using the full CDF Run II data set, which corresponds to an integrated luminosity of 9.1 fb^{-1} from 1.96 TeV $p\bar{p}$ collisions. The result is $M_{\text{top}} = 171.5 \pm 1.9 \text{ (stat)} \pm 2.5 \text{ (syst)} \text{ GeV}/c^2$. The measured value of M_{top} is compatible with the world-average top-quark mass of $M_{\text{top}} = 173.34 \pm 0.76 \text{ GeV}/c^2$ [3]. This measurement is the final CDF Run II result in the dilepton channel and supersedes the previous published value of $M_{\text{top}} = 170.3 \pm 2.0 \text{ (stat)} \pm 3.1 \text{ (syst)} \text{ GeV}/c^2$ [6]. The accuracy achieved is approximately 14% better than in the previous measurement. Most of this improvement, 9%, is due to using a new technique for optimizing the combined statistical and systematic uncertainty while the rest, 5%, is due to using a larger data sample. This technique is applicable to a wide range of measurements whose precisions are dominated by systematic uncertainties, in which an optimization between statistical and systematic uncertainty is required.

ACKNOWLEDGMENTS

We thank the Fermilab staff and the technical staffs of the participating institutions for their vital contributions. This work was supported by the U.S. Department of Energy and National Science Foundation; the Italian Istituto Nazionale di Fisica Nucleare; the Ministry of Education, Culture, Sports, Science and Technology of Japan; the Natural Sciences and Engineering Research Council of Canada; the National Science Council of the Republic of China; the Swiss National Science Foundation; the A.P. Sloan Foundation; the Bundesministerium für Bildung und Forschung, Germany; the Korean World Class University Program, the National Research Foundation of Korea; the Science and Technology Facilities Council and the Royal Society, United Kingdom; the Russian Foundation for Basic Research; the Ministerio de Ciencia e Innovación, and Programa Consolider-Ingenio 2010, Spain; the Slovak R&D Agency; the Academy of Finland; the Australian Research Council (ARC); and the EU community Marie Curie Fellowship Contract No. 302103.

- [1] M. Baak, M. Goebel, J. Haller, A. Hoecker, D. Kennedy, R. Kogler, K. Moenig, M. Schott, and J. Stelzer, *Eur. Phys. J. C* **72**, 2205 (2012).
- [2] D. Buttazzo, G. Degrossi, P. P. Giardino, G. F. Giudice, F. Sala, A. Salvio, and A. Strumia, *J. High Energy Phys.* **12** (2013) 089.
- [3] G. Aad *et al.* (ATLAS, CDF, CMS, and D0 Collaborations), arXiv:1403.4427.
- [4] T. Aaltonen *et al.* (CDF and D0 Collaborations), arXiv:1407.2682.
- [5] K. A. Olive *et al.* (Particle Data Group), *Chin. Phys. C* **38**, 090001 (2014).
- [6] T. Aaltonen *et al.* (CDF Collaboration), *Phys. Rev. D* **83**, 111101 (2011).
- [7] V. M. Abazov *et al.* (D0 Collaboration), *Phys. Rev. D* **86**, 051103 (2012).
- [8] T. Aaltonen *et al.* (CDF Collaboration), *Phys. Rev. Lett.* **109**, 152003 (2012).
- [9] T. Aaltonen *et al.* (CDF Collaboration), *Phys. Lett. B* **714**, 24 (2012).
- [10] T. Aaltonen *et al.* (CDF Collaboration), *Phys. Rev. D* **88**, 011101 (2013).
- [11] T. Aaltonen *et al.* (CDF Collaboration), *Phys. Rev. D* **81**, 032002 (2010).
- [12] T. Aaltonen *et al.* (CDF Collaboration), *Phys. Lett. B* **698**, 371 (2011).
- [13] D. Acosta *et al.* (CDF Collaboration), *Phys. Rev. D* **71**, 032001 (2005).
- [14] A cylindrical (r, ϕ, z) coordinate system is used. The origin of the reference system is the geometric center of the detector, with the z axis pointing along the proton beam. The pseudorapidity η is defined by $\eta = -\ln(\tan(\theta/2))$, where θ is the polar angle relative to the z axis. The transverse momentum and energy of a detected particle or jet are defined as $p_T = p \sin \theta$ and $E_T = E \sin \theta$, respectively, where p and E are the momentum and energy of the particle or jet.
- [15] T. Aaltonen *et al.* (CDF Collaboration), *Phys. Rev. D* **88**, 091103 (2013).
- [16] A lepton is isolated when the transverse energy measured in the calorimeter not associated with the lepton and calculated in a cone of radius $\Delta R = \sqrt{\Delta\eta^2 + \Delta\phi^2} = 0.4$ about the lepton trajectory does not exceed 10% of the lepton E_T (p_T for muons).
- [17] The missing transverse energy, an imbalance of energy in the transverse plane of the detector, is defined by $\cancel{E}_T = |-\sum_i E_T^i \hat{n}_i|$ where the sum is performed over the calorimeter towers. The quantity \hat{n}_i is the unit vector normal to the beam and pointing from the interaction vertex to the i th tower. The \cancel{E}_T for events with identified muons is corrected by the measured muon transverse momentum.
- [18] F. Abe *et al.* (CDF Collaboration), *Phys. Rev. D* **45**, 1448 (1992).
- [19] A. Bhatti *et al.*, *Nucl. Instrum. Methods Phys. Res., Sect. A* **566**, 375 (2006).
- [20] The variable named E_T significance is defined as $\cancel{E}_T/\sqrt{E_T^{\text{sum}}}$. The value of E_T^{sum} is calculated as the sum of transverse energies deposited in calorimeter towers and is corrected for the muon transverse momenta, if muons are identified, and various other instrumental effects.
- [21] H_T is defined as the transverse-energy scalar sum over leptons, jets, and \cancel{E}_T .
- [22] D. Acosta *et al.* (CDF Collaboration), *Phys. Rev. D* **71**, 052003 (2005).
- [23] T. Sjöstrand, S. Mrenna, and P. Skands, *J. High Energy Phys.* **05** (2006) 026.
- [24] H. L. Lai, J. Huston, S. Kuhlmann, J. Morfin, F. Olness, J. F. Owens, J. Pumplin, and W. K. Tung, *Eur. Phys. J. C* **12**, 375 (2000).
- [25] E. Gerchtein and M. Paulini, arXiv:physics/0306031.
- [26] M. L. Mangano, M. Moretti, F. Piccinini, R. Pittau, and A. D. Polosa, *J. High Energy Phys.* **07** (2003) 001.
- [27] T. Aaltonen *et al.* (CDF Collaboration), *Phys. Rev. D* **79**, 092005 (2009).
- [28] T. Affolder *et al.* (CDF Collaboration), *Phys. Rev. D* **63**, 032003 (2001).
- [29] T. Aaltonen *et al.* (CDF Collaboration), *Phys. Rev. D* **79**, 072005 (2009).
- [30] A. Abulencia *et al.* (CDF Collaboration), *Phys. Rev. D* **73**, 112006 (2006).
- [31] G. Corcella, I. G. Knowles, G. Marchesini, S. Moretti, K. Odagiri, P. Richardson, M. H. Seymour, and B. R. Webber, *J. High Energy Phys.* **01** (2001) 010.
- [32] P. Z. Skands and D. Wicke, *Eur. Phys. J. C* **52**, 133 (2007).
- [33] J. Pumplin, D. R. Stump, J. Huston, H. L. Lai, P. Nadolsky, and W. K. Tung, *J. High Energy Phys.* **07** (2002) 012.
- [34] T. Aaltonen *et al.* (CDF and D0 Collaborations), *Phys. Rev. D* **86**, 092003 (2012).